

Generation and manipulation of isotropic droplets in nematic medium using switchable dielectrophoresis

Bomi Lee¹, Jun-Seo Lee¹, Hyun-Jin Yoon^{1,2}, Seung-Ho Hong¹, and Jang-Kun Song^{1,*}

¹*Department of Electrical & Computer Engineering, Sungkyunkwan University, Suwon, Gyeonggi-do 16419, Republic of Korea*

²*Merck Performance Materials Ltd., Pyeongtaek 17956, Republic of Korea*



(Received 20 September 2019; published 31 January 2020)

Dielectrophoresis (DEP) in a medium with anisotropic dielectric susceptibility is very different from typical DEP in an isotropic medium: The direction of particle actuation can be switched depending on the direction of the susceptibility tensor of the medium. However, the understanding of switchable DEP (SDEP) in an anisotropic medium is still in its infant stage. Here, we investigate SDEP using heat-generated isotropic droplets in a nematic liquid crystal (LC) medium. We demonstrate that the location of the generation of isotropic droplets can be partially controlled by controlling the temperature gradient within the LC cell using dielectric loss. The SDEP actuation of isotropic droplets is also highly dependent on the location of the isotropic droplets. Using this method, we fabricated different array patterns of isotropic and nematic phase separations under different applied signals.

DOI: [10.1103/PhysRevE.101.012704](https://doi.org/10.1103/PhysRevE.101.012704)

I. INTRODUCTION

Dielectrophoresis (DEP), the propelling motion of a neutral particle within a nonuniform electric field, is attributed to the imbalanced Lorenz forces induced by the nonuniform electric field [1–3]. The DEP force (\mathbf{F}_{DEP}) is expressed by the gradient of the square of the electric field (∇E^2) and relative dielectric constant of particle and medium (ϵ_p and ϵ_m) as

$$\mathbf{F}_{\text{DEP}} = 2\pi\epsilon_0\epsilon_m R^3 \left(\frac{\epsilon_p - \epsilon_m}{\epsilon_p + 2\epsilon_m} \right) \nabla E^2, \quad (1)$$

where ϵ_0 and R are the vacuum permittivity and the radius of the spherical particle, respectively. Hence, depending on the sign of $(\epsilon_p - \epsilon_m)$, the \mathbf{F}_{DEP} can be along or opposite to the direction of ∇E^2 , referred to as positive or negative DEP, respectively [4]. DEP has been widely studied to manipulate or sort small particles in a medium and has been used in a variety of fields such as micro- or nanoscience [5–8], biomedical [9–11], and chemical engineering [12]. However, there is a well-known limitation of DEP; it has a one-way impetus characteristic along the ∇E^2 , and it cannot actuate particles to any other direction.

Recently, we reported a very unique way to overcome the limitation, that is, switchable dielectrophoresis (SDEP) in a special biphasic liquid crystal (LC) system that consists of an anisotropic nematic LC medium and isotropic LC droplets [13,14]. The isotropic droplets, which have basically the same chemical composition as the nematic medium, can exist within a narrow temperature range in a nematic LC mixture [15–18]. By controlling the temperature, the number and size of isotropic LC droplets can be controlled. In particular, defect-free LC alignment is obtained around the isotropic

droplets because the isotropic droplet surface has very weak surface anchoring energy for LC alignment [13,19,20].

The unique physical properties of SDEP can be summarized as follows:

(1) The direction of the SDEP force is not parallel to the squared field gradient (∇E^2), which clearly distinguishes SDEP from conventional DEP.

(2) The force direction of SDEP is controlled by the LC director direction, that is, the particle migration direction can be changed to any direction by controlling the LC director direction.

(3) The SDEP phenomenon can be modeled by introducing the tensor form of dielectric susceptibility difference between the nematic medium and the isotropic droplet.

We also demonstrated the use of isotropic droplets as cargo carriers of nanoparticles or microparticles by combining the SDEP phenomenon [13] with the solubility contrast of nano- or microparticles in nematic and isotropic phases [21–23]. Using this method, we successfully fabricated a point-light-source array made of quantum dots [24]. DEP applications for manipulating nano- or microparticles have several advantages compared to electrophoretic devices [25,26] or mechanical microfluidic devices [27–29]. DEP force can be applied to both neutral particles and charged particles [4,30–32], and it does not require bulky mechanical components. By overcoming the one-way impetus characteristic of DEP applications using the SDEP concept, one may be able to fully utilize the advantages of DEP devices. In particular, by combining with microfluidic technology [33–37] and optimizing the electrode design and electric signals in SDEP devices, much effective sorting and separation of biological materials or cells may be achievable within a programmable SDEP chip, although many challenging issues still remain to be solved.

The SDEP is, thus, significantly different from the typical DEP phenomenon [1–3], and is also an interesting and useful

*jk.song@skku.edu

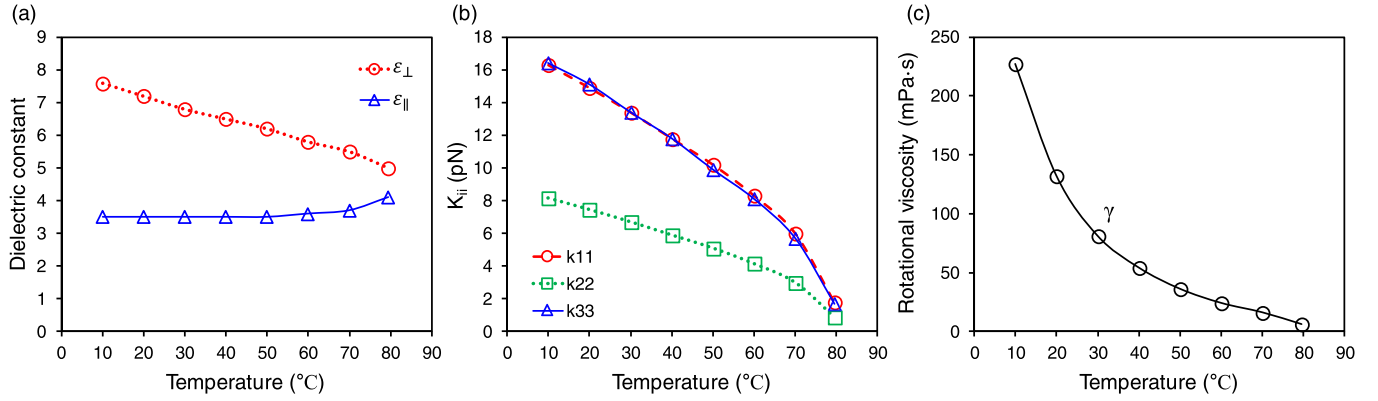


FIG. 1. (a) Perpendicular (ϵ_{\perp}) and parallel (ϵ_{\parallel}) dielectric constant at 60 Hz, (b) elastic constants, and (c) rotational viscosity of MLC-7026-000 as a function of temperature.

tool to control small objects [13]. However, the understanding of SDEP is still in its infancy and requires further study. In this study, we clarify three aspects of SDEP. First, the generation of isotropic droplets is not a well-controlled process. In previous experiments, we simply heated an LC cell to near nematic-to-isotropic transition temperature (T_{NI}) to create many isotropic droplets. Then, we selected one droplet in the right position to investigate the SDEP phenomenon. Second, the SDEP force distribution is quite complex in the cell containing orthogonally interlaced electrodes used in our previous experiments. The migration direction of the droplet must be highly dependent on the location of the isotropic droplet. However, in our previous experiments, we analyzed the droplet motion only along a small segment on the electrode. How does the SDEP force behave in other areas of the cell? Lastly, the dependence of isotropic droplet size on the SDEP has not been discussed. When an isotropic droplet grows large, its shape and location can be influenced by the nonuniform SDEP force and surface tension. To study the above three aspects of SDEP, we analyze the SDEP phenomenon under different applied voltages. Interestingly, the isotropic droplets appeared at different locations and followed different moving trajectories depending on the applied volt-

age. The results will extend our understanding of the SDEP phenomenon.

II. EXPERIMENT AND SIMULATION

A. LC material, cell structure, and electric field distribution

A commercial negative LC mixture MLC-7026-000 (Merck Co., Korea) was used in the experiment. Its scalar dielectric anisotropy ($\delta\epsilon$) is -3.9 at 20°C and 1 kHz electric fields. $\delta\epsilon$ is almost constant in the frequency range of 10 Hz – 1 kHz [13], but it is sensitively dependent on the temperature [Fig. 1(a)] and it becomes ~ -0.9 near the phase transition temperature (79°C). Similarly, the elastic constants are also sensitively dependent on the temperatures, and $K_{11} \sim 1.8$, $K_{33} \sim 1.7$ at 79°C , as shown in Fig. 1(b). The rotational viscosity (γ) is shown in Fig. 1(c) and it becomes $\sim 6\text{ mPa}\cdot\text{s}$ at 79°C . These LC properties at 79°C were used in our simulation. In general, K_{22} is roughly half of K_{11} , and K_{22} is approximated to be -0.9 in the simulation. The details of material parameters of LC are given in Table I.

Glass substrates with interdigitated strip electrodes of indium tin oxide were prepared. The width and distance of the strip electrodes were 10 and $50\text{ }\mu\text{m}$, respectively. A

TABLE I. The specific property parameters of LC, ITO, alignment layer used in TECHWIZ.

Layer name	Material	Thickness	Dielectric constants	Refractive indices	Miscellaneous
Top substrate	Glass	$15\text{ }\mu\text{m}$	7	1.5	–
Electrode	ITO	$0.035\text{ }\mu\text{m}$	–	1.81	–
Electrode	ITO	$0.035\text{ }\mu\text{m}$	–	1.81	–
Alignment	PI	$0.1\text{ }\mu\text{m}$	3.8	1.68	Top pretilt: 90° Strong anchoring
LC	MLC-7026-000	$6.5\text{ }\mu\text{m}$	$\epsilon_{\perp} = 5$ $\epsilon_{\parallel} = 4.1$	$N_e = 1.5577$ $N_o = 1.4755$	$K_{11} = 1.8\text{ pN}$ $K_{22} = 0.9\text{ pN}$ $K_{33} = 1.7\text{ pN}$ $\gamma = 6\text{ mPa}\cdot\text{s}$
Alignment	PI	$0.1\text{ }\mu\text{m}$	3.8	1.68	Bottom pretilt: 90° Strong anchoring
Electrode	ITO	$0.035\text{ }\mu\text{m}$	–	1.81	–
Electrode	ITO	$0.035\text{ }\mu\text{m}$	–	1.81	–
Bottom substrate	Glass	$15\text{ }\mu\text{m}$	7	1.5	–

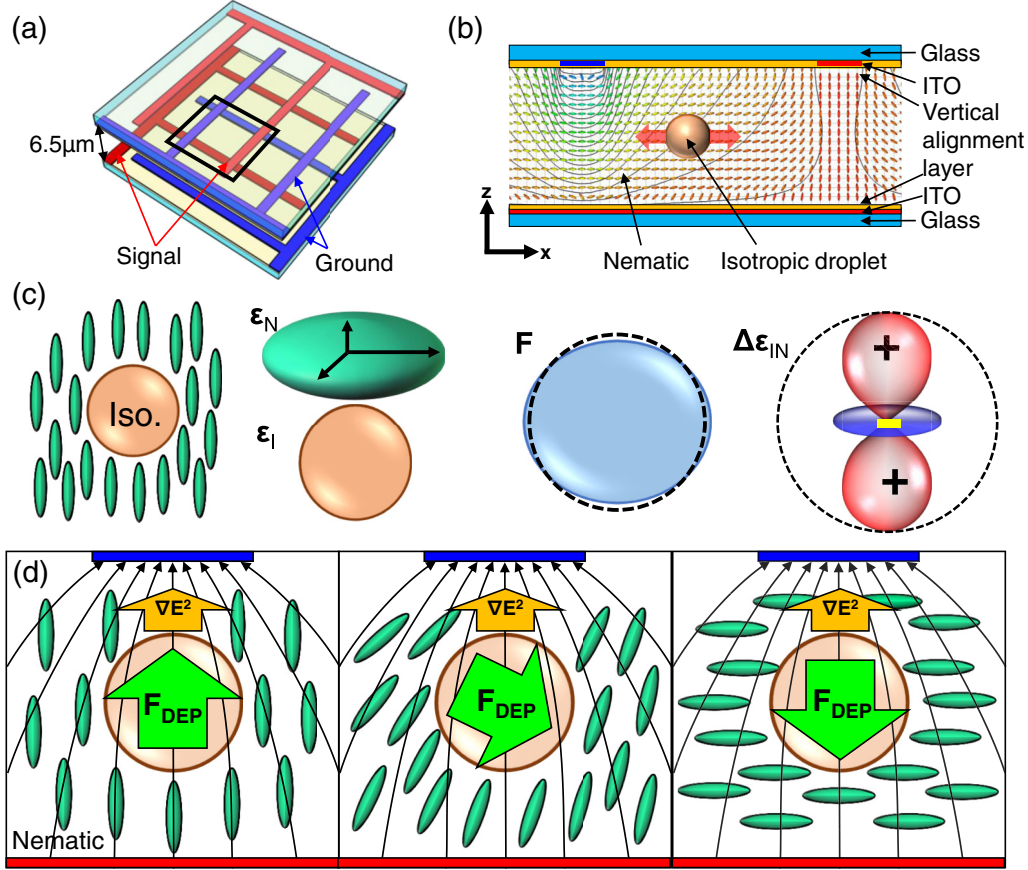


FIG. 2. (a) The LC cell configuration. The width of electrodes and their interspace are 10 and 50 μm , respectively. (b) Equipotential lines and LC director distribution at the cross section of the cell under the application of a 10-V, 60-Hz square-wave signal. (c) Tensor coefficient \mathbf{F} and permittivity difference tensor ($\Delta\epsilon_{IN}$) between ϵ_I and ϵ_N . (d) Schematics for the variation of \mathbf{F}_{SDEP} direction depending on the LC director.

commercial polyimide solution AL60101 (JSR Company, Japan) was spin coated onto the substrate. Then, LC cells were fabricated by orthogonally overlapping two substrates with the interdigitated strip electrodes, as shown in Fig. 2(a). The thickness of the LC cell was approximately 6.5 μm . Then, LC was injected into the LC cell by capillary action.

To induce a nonuniform electric field inside the LC cell, a 60-Hz square-shaped alternating current signal was applied to the substrates, as shown in Fig. 2(a). Highly nonuniform electric field distribution was obtained, as shown in the cross-sectional diagram for the equipotential lines in Fig. 2(b). As a result, the LC director profile also varied according to the location in the cell.

B. SDEP model using dielectric susceptibility tensor

The total energy potential (ΔU_{total}) of a defect-free isotropic droplet can be written as [13]

$$\begin{aligned}\Delta U_{\text{total}} &= \frac{1}{2}\epsilon_0 \int (\mathbf{E}_I \cdot \epsilon_N \mathbf{E}_N - \mathbf{E}_N \cdot \epsilon_I \mathbf{E}_I) dV \\ &= \frac{1}{2}\epsilon_0 \int [\mathbf{E}_I \cdot (\epsilon_I - \Delta\epsilon_{IN}) \mathbf{E}_N - \mathbf{E}_N \cdot \epsilon_I \mathbf{E}_I] dV \\ &= \frac{1}{2}\epsilon_0 \int [\epsilon_I (\mathbf{E}_I \cdot \mathbf{E}_N - \mathbf{E}_N \cdot \mathbf{E}_I) - \mathbf{E}_I \cdot \Delta\epsilon_{IN} \mathbf{E}_N] dV \\ &= -\frac{1}{2}\epsilon_0 \int [\mathbf{E}_I \cdot \Delta\epsilon_{IN} \mathbf{E}_N] dV,\end{aligned}\quad (2)$$

where ϵ_I , ϵ_N , \mathbf{E}_N , and \mathbf{E}_I are the relative tensor permittivity of isotropic and nematic phases, the electric field distribution inside the nematic medium and isotropic droplet, respectively, and $\Delta\epsilon_{IN} = (\epsilon_I - \epsilon_N)$. The relationship between \mathbf{E}_I and \mathbf{E}_N can be expressed as

$$\begin{aligned}\mathbf{E}_I &= [3\epsilon_N(\epsilon_I + 2\epsilon_N)^{-1}] \mathbf{E}_N \equiv \mathbf{F} \mathbf{E}_N \\ &\simeq \frac{3\epsilon_N}{\epsilon_I + 2\epsilon_N} \mathbf{E}_N \equiv f \mathbf{E}_N.\end{aligned}\quad (3)$$

Owing to the small $\delta\epsilon$ near T_{NI} , the angular variation of the tensor coefficient \mathbf{F} is negligible, as illustrated in Fig. 2(c), and the scalar approximation in Eq. (3) is valid. Then, ΔU_{total} of a defect-free isotropic droplet with the volume V can be further simplified as

$$\begin{aligned}\Delta U_{\text{total}} &= -\frac{1}{2}\epsilon_0 \int [\mathbf{F} \mathbf{E}_N \cdot \Delta\epsilon_{IN} \mathbf{E}_N] dV \\ &\simeq -\frac{1}{2}\epsilon_0 f V \mathbf{E}_N \cdot \Delta\epsilon_{IN} \mathbf{E}_N,\end{aligned}\quad (4)$$

where $\Delta\epsilon_{IN}$ can be expressed using the Euler angle rotational matrix $\mathbf{R}(\varphi, \theta)$ as

$$\Delta\epsilon_{IN} = \frac{1}{3} \mathbf{R}(\varphi, \theta) \begin{pmatrix} \delta\epsilon & 0 & 0 \\ 0 & \delta\epsilon & 0 \\ 0 & 0 & -2\delta\epsilon \end{pmatrix} \mathbf{R}(\varphi, \theta)^T. \quad (5)$$

In Eq. (4), it is assumed that V is small and \mathbf{E} is more or less constant within the isotropic droplet. Then, the SDEP force (\mathbf{F}_{SDEP}) can be expressed in tensor form as [13]

$$\begin{aligned}\mathbf{F}_{\text{SDEP}} &= -\nabla(\Delta U_{\text{total}}) \simeq \frac{1}{2}\epsilon_0 V \nabla[(\mathbf{F}\mathbf{E}) \cdot (\Delta\epsilon_{\text{IN}}\mathbf{E})] \\ &\simeq \frac{1}{2}\epsilon_0 V f \nabla[\mathbf{E} \cdot (\Delta\epsilon_{\text{IN}}\mathbf{E})].\end{aligned}\quad (6)$$

$\Delta\epsilon_{\text{IN}}$ is determined by the LC director orientation described by azimuthal (φ) and polar angles (θ), as illustrated in Fig. 2(c); the red colors along the polar direction and blue colors along the equator direction indicate the positive and negative values of $\Delta\epsilon_{\text{IN}}$. The rotational symmetric axis of $\Delta\epsilon_{\text{IN}}$ is parallel to the LC director (\mathbf{n}); hence, the direction of $\Delta\epsilon_{\text{IN}}$ can rotate when \mathbf{n} is switched, producing the switchable \mathbf{F}_{SDEP} . The switchable \mathbf{F}_{SDEP} is briefly explained using simplified illustrations in Fig. 2(d); when the applied voltage increases, the director direction can be changed as shown in the three cases in Fig. 2(d). In our experiment, $\delta\epsilon$ (~ -0.9) of the LC near T_{NI} is small compared to the dielectric constants of the LC, which are 4.1 and 5 along and perpendicular to the director, respectively. As a result, the rotation of the director does not result in meaningful change of the directions of \mathbf{E} and $\nabla\mathbf{E}^2$, which will be discussed further in the next section. However, when the LC director changes from vertical to horizontal, $\Delta\epsilon_{\text{IN}}$ rotates accordingly. As a result, the \mathbf{F}_{SDEP} rotates as well. When the LC director rotates 90° , \mathbf{F}_{SDEP} rotates by almost twice as much [13].

The LC director and \mathbf{E} profiles in the LC cell distribution were simulated using the commercial software TECHWIZ 3D, designed specifically for LC director simulation. The simulation conditions are $\delta\epsilon = -0.9$, $K_{11} = 1.8$, $K_{22} = 0.9$, $K_{33} = 1.7$, and $\gamma = 6 \text{ mPa s}$. The cell configuration used in the simulation is given in Table I. Then, using the LC director and \mathbf{E} profiles acquired through TECHWIZ, the \mathbf{F}_{SDEP} and ΔU_{total} were calculated by Eqs. (4) and (6) [13]. In these calculations, the size of the droplet was assumed to be a fixed value, $10 \mu\text{m}$.

III. RESULTS AND DISCUSSION

A. Simulation results

The LC director profile, electric field profile, and $\nabla\mathbf{E}^2$ profile within a cell were simulated using the material and cell parameters in Table I and the simulation procedure described in the previous section. The results are shown in Figs. 3–5. Figure 3 shows the LC director profile within a periodic unit in the cell shown in Fig. 2(a). In the left image of Fig. 3(a), H and L indicate the cross points of electrodes with the highest and lowest electric fields, respectively, and M is the center of the compartment made of stripe electrodes. The right image in Fig. 3(a) shows the LC director distribution profile along the electrode at 15, 30, and 50 V, respectively. The LC director changes significantly as the applied voltage increases, as well indicated in the black boxes. On the other hand, the LC director profiles along the diagonal direction shown in Fig. 3(b) do not show meaningful variation with the increasing voltage.

Figure 4 shows the normalized \mathbf{E} fields at 15, 30, and 50 V. Figures 4(a), 4(b), and 4(c) show the top view, and cross-sectional views along the electrode and the diagonal direction, respectively. Here, the background color indicates the normalized strength of \mathbf{E} , that is, $\mathbf{E}/\mathbf{E}_{\text{max}}$, where \mathbf{E}_{max}

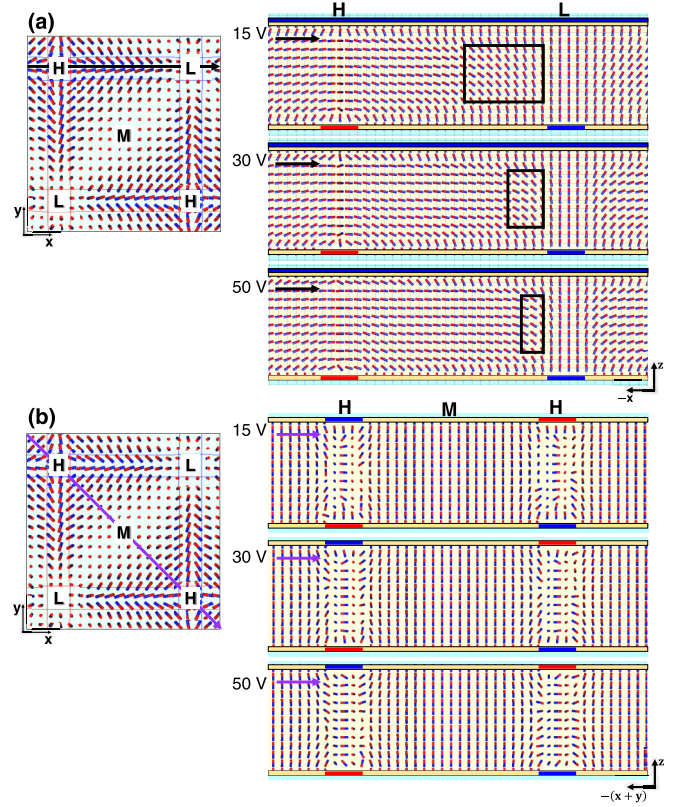


FIG. 3. (a) The cross-sectional views of the LC director profile along the electrode (black line) and (b) along the diagonal direction (purple line) at 15, 30, and 50 V, respectively. The LC director distribution along the electrode dramatically changes depending on the applied voltages [see the black squares in (a)], but the variation of the LC director along the diagonal direction is small, as shown in (b).

is the maximum electric field strength in each case. \mathbf{E}_{max} is approximately 1.6, 3.3, and 5.5 $\text{V}/\mu\text{m}$, at 15, 30, and 50 V, respectively. The large difference of the normalization factor, \mathbf{E}_{max} , indicates the large difference in the magnitude of electric fields in the three cases. However, as shown in Fig. 4, the normalized \mathbf{E} is almost unchanged with the increasing voltage. It is expected that the variation of the LC director profile may cause the change of the \mathbf{E} field profile owing to the variation of the effective dielectric constant of the LC. However, the variation of the effective dielectric constant of the LC is very small owing to the small $\delta\epsilon$ near T_{NI} . As a result, the normalized \mathbf{E} is almost unchanged in the cell.

A similar result is obtained in the normalized $\nabla\mathbf{E}^2$ profile shown in Fig. 5, where the top view and the cross-sectional views of the normalized $\nabla\mathbf{E}^2$ along the electrode and the diagonal direction are shown. Here, the normalized $\nabla\mathbf{E}^2$ means $\nabla\mathbf{E}^2/\nabla\mathbf{E}_{\text{max}}^2$, and $\nabla\mathbf{E}_{\text{max}}^2$ is approximately 9×10^{17} , 3×10^{18} , and $1 \times 10^{19} \text{ V}^2/\text{m}^3$, at 15, 30, and 50 V, respectively. Although the magnitude of $\nabla\mathbf{E}^2$ increases sharply, the overall normalized profile is unchanged.

B. SDEP at 15 V

An LC cell was slowly heated close to T_{NI} with the application of 15 V, and isotropic droplets (depicted as white

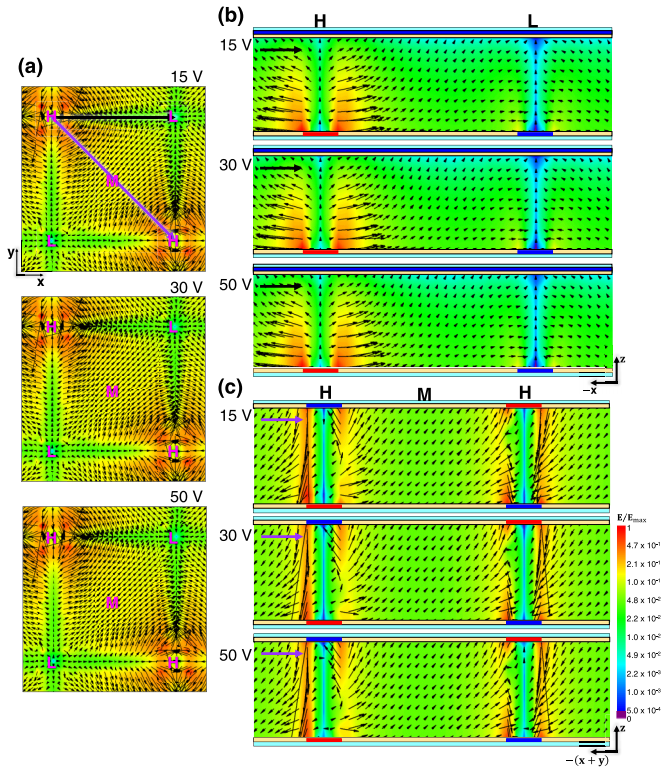


FIG. 4. (a) The top view, and (b) the cross-sectional views of normalized \mathbf{E} (that is, \mathbf{E}/E_{\max}) fields along the electrode [black line at (a)], and (c) along the diagonal direction [purple diagonal line at (a)] at 15, 30, and 50 V, respectively. The normalized \mathbf{E} is not changed significantly. E_{\max} is 1.6, 3.3, and 5.5 V/ μm , at 15, 30, and 50 V, respectively.

dot circles) started to appear, as shown in Fig. 6(a). The isotropic droplets appeared in random locations, but only a few were generated near H, where an umbilic defect existed. Once many small isotropic droplets were generated, they grew in size and the number of newly generated droplets reduced dramatically. Then, the isotropic droplets moved along the yellow dotted arrows in Fig. 6(b), and some merged when they approached close to each other. The overall direction of droplet migration was mostly away from the H points. The detailed dynamic motion can be seen in Supplemental Video S1 in the Supplemental Material [38]. Roughly 1 min later, the migration motion almost stopped, and the final locations of the isotropic droplets are shown in Fig. 6(c). The location of isotropic droplets can be categorized into two types: A_1 , marked by blue dotted circles located in the middle of the electrode line, and B_1 , marked by red solid circles in the center of the compartments.

The SDEP was analyzed for one periodic unit of the electrode structures [the white square in Fig. 6(b)]. The top view and cross-sectional views of LC director distribution are precisely described in Figs. 6(d) and 3, respectively. The $\nabla \mathbf{E}^2$ profile is plotted in Fig. 6(e), in which the direction and magnitude of $\nabla \mathbf{E}^2$ are represented by arrows and background colors, respectively. The L and H points become the sources and sinks for $\nabla \mathbf{E}^2$ vector fields, and $\nabla \mathbf{E}^2$ vectors are directed from L to H. In the typical DEP phenomenon in an isotropic medium, the direction of the DEP force is always parallel to

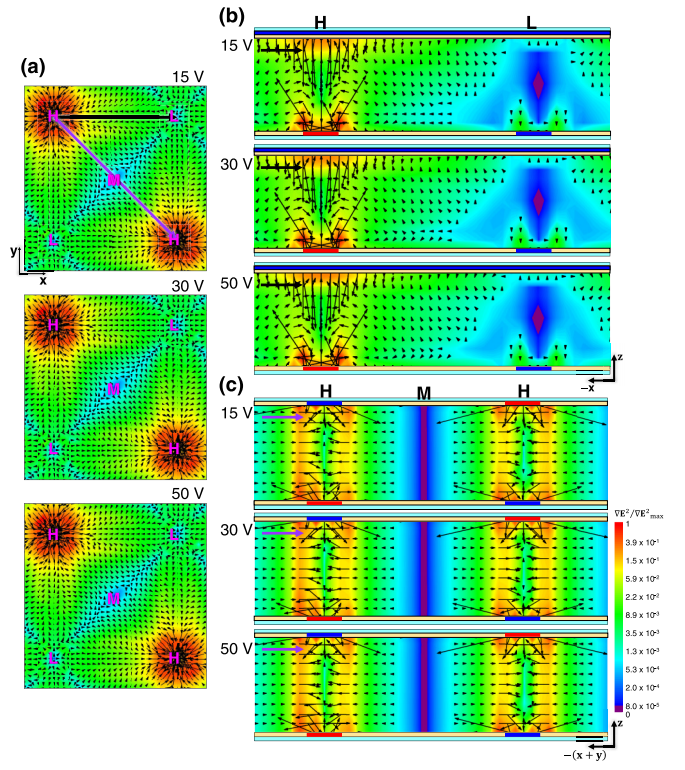


FIG. 5. (a) The top view, and (b) the cross-sectional views of the normalized $\nabla \mathbf{E}^2$ (that is, $\nabla \mathbf{E}^2/\nabla \mathbf{E}^2_{\max}$) along the electrode [black line at (a)], and (c) along the diagonal direction [purple diagonal line at (a)] at 15, 30, and 50 V, respectively. The normalized magnitude of $\nabla \mathbf{E}^2$, that is, $\nabla \mathbf{E}^2/\nabla \mathbf{E}^2_{\max}$, is expressed by the background color. $\nabla \mathbf{E}^2_{\max}$ is approximately 9×10^{17} , 3×10^{18} , and 1×10^{19} V²/m³, at 15, 30, and 50 V, respectively.

$\nabla \mathbf{E}^2$, which means that an object within the field distribution shown in Fig. 6(e) should move to the H or L position depending on the sign of the relative dielectric difference between the object and medium [4,39,40]. However, the locations of isotropic droplets in Fig. 6(c) are totally different from those expected in typical DEP, which can be explained by the SDEP. Figure 6(f) shows the \mathbf{F}_{SDEP} vector fields (arrows) and the magnitude of ΔU_{total} (the background color), respectively. The difference between $\nabla \mathbf{E}^2$ and \mathbf{F}_{SDEP} vector fields is well indicated by comparing the boxes in Figs. 6(e) and 6(f). The $\nabla \mathbf{E}^2$ vector fields are directed from right to left [Fig. 6(e)], but \mathbf{F}_{SDEP} vector fields in the same area have a singular point in the middle, where the isotropic droplets are gathered. Thus, the locations of A_1 -type isotropic droplets are well explained by \mathbf{F}_{SDEP} analysis. Near the singularity point, the LC director directions dramatically vary as a function of position as shown in Fig. 3, indicating that the abrupt change of \mathbf{F}_{SDEP} direction at the singularity is related to the LC director direction.

However, the locations of B_1 -type droplets cannot be explained by such analysis. The color in Fig. 6(g) represents the magnitude of \mathbf{F}_{SDEP} ; in the M position, \mathbf{F}_{SDEP} is the weakest. \mathbf{F}_{SDEP} is roughly 94.55 and 2.39 pN at the centers of the A_1 circle in Fig. 6(f) and the B_1 circle in Fig. 6(g), respectively; that is, \mathbf{F}_{SDEP} at A_1 -type isotropic droplets is approximately 40 times larger than that at the B_1 -type droplets. In our previous

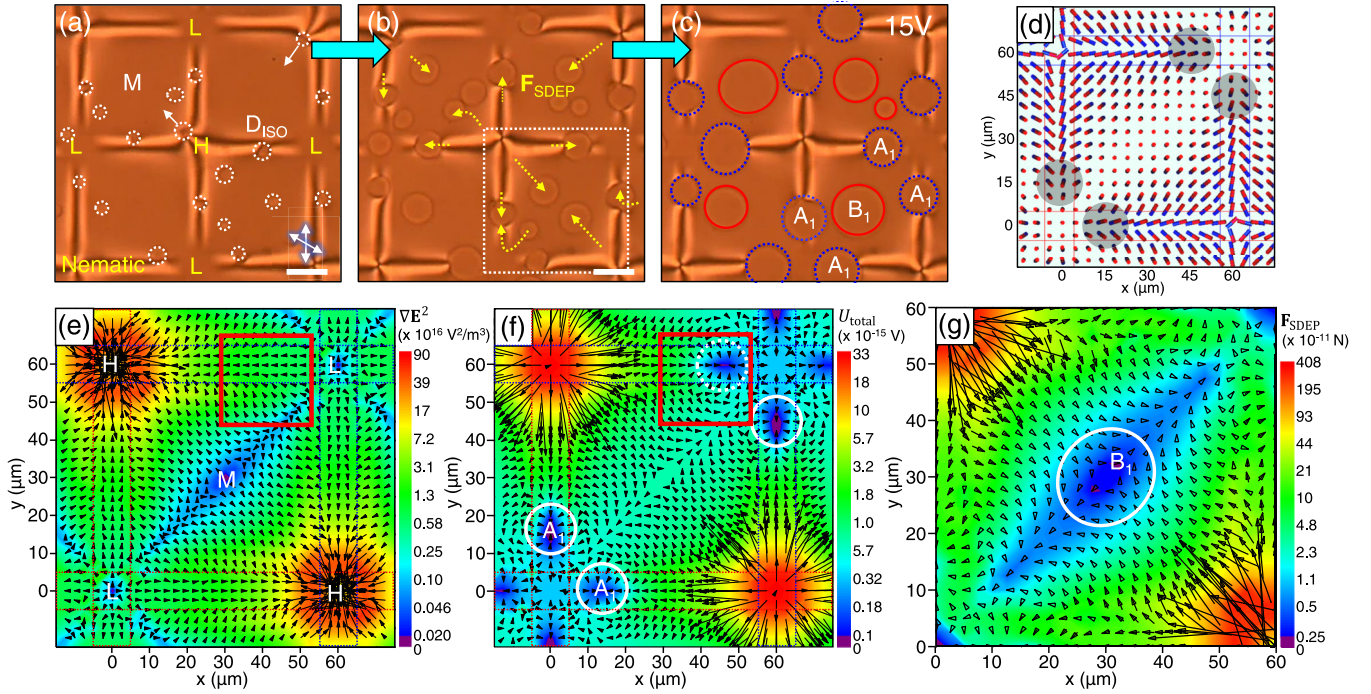


FIG. 6. (a–c) Procedure of generation, migration, and growth of isotropic droplets at 15 V. (a) Isotropic droplets are randomly generated near T_{NI} . (b) Yellow dotted line indicates the migration of the droplets by \mathbf{F}_{SDEP} . (c) After 58 s, the isotropic droplets are located either on the middle of the electrode (A_1 type) or around M (B_1 type). (d) LC director profile. (e) ∇E^2 profile. (f) \mathbf{F}_{SDEP} vector fields (arrows) and ΔU_{total} profile (background color). (g) \mathbf{F}_{SDEP} vector field profile (arrows) and the magnitude of \mathbf{F}_{SDEP} (background color). Scale bars, 20 μm .

report, particle actuation using SDEP has a hysteresis, indicating the presence of friction in the motion of isotropic droplets [13]. Hence, the weak SDEP cannot actuate the isotropic droplets. In addition, the symmetric force fields in the M point reduce the net SDEP force to drag the droplets. The surface integration of SDEP along the droplet surface provides the net force to drag the droplet, and the mirror symmetric force field shown in Fig. 6(g) brings about much weaker net force for the isotropic droplets.

C. SDEP at 30 V

With the application of 30 V, very different behaviors of isotropic droplets were observed. Most isotropic droplets were generated near the H points, the area marked by the white dotted circle ($\sim 15 \mu\text{m}$ radius) in Fig. 7(a). The generated isotropic droplets radially spread out [Fig. 7(b)] and then merged together. The number of newly generated droplets dramatically decreased over time, while the generated droplets grew, similar to the case at 15 V (see Supplemental Video S2 [38]).

After approximately 46 s, all the droplets aligned diagonally, and some droplets marked A_2 were located at the L points, as shown in Fig. 7(c). The LC director profile within a periodic unit area is shown in Figs. 7(d) and 3. It is clearly shown that the rapidly varying LC director area shifted toward the L point compared to the case of 15 V application [see the boxes in Fig. 3(a)]. The \mathbf{F}_{SDEP} profile shown in Fig. 7(e), where the arrows and colors represent the direction of \mathbf{F}_{SDEP} and the magnitude of ΔU_{total} , respectively, clearly explains the droplet distribution. \mathbf{F}_{SDEP} pushes the droplets toward the diagonal lines where the droplets are located, as shown

in Fig. 7(c). Although the lowest DEP potential is located at the L points [Fig. 7(e)], the driving force from M point to L point is very weak, and the droplets are located along the diagonal lines with the lowest DEP force. The color in Fig. 7(f) shows the magnitude of \mathbf{F}_{SDEP} , indicating the weakest DEP force along the diagonal direction. Along the electrodes, the minimum DEP potential was found at the L points, which is different from the case of 15 V application. As a result, no droplet exists in the middle of the electrodes [compare A_1 in Fig. 6(c) and A_2 in Fig. 7(c)].

Close observation of droplet migration reveals the trajectories of the droplets (Fig. 7(g) and Supplemental Video S2 [38]). The droplets generated in the middle of the H points or on top of electrodes migrated along the electrode and merged at the L points, producing the A_2 droplets. On the other hand, the droplets generated outside the electrode (or the peripheral area of the electrodes) moved toward the middle of the diagonal lines, producing the B_2 droplets marked by red solid circles in Fig. 7(c). Thus, A_2 and B_2 droplets grew by merging with small droplets generated at different locations. The droplets generated near the periphery of the electrodes followed parabolic trajectories, shown in the white solid line Fig. 7(g). The parabolic trajectory coincided with the direction of \mathbf{F}_{SDEP} in Fig. 7(e).

The \mathbf{F}_{SDEP} profiles at 15 and 30 V look similar, as shown in Figs. 6(g) and 7(f), but the shapes of B_1 s at 15 V and B_2 s at 30 V are rather different; B_1 s are likely to form a large single droplet at the M point [Fig. 6(c)] and B_2 s are usually a chain of small droplets [Fig. 7(c)]. As shown in the precise comparisons of \mathbf{E} and ∇E^2 between the cases of 15 and 30 V applications in Figs. 4 and 5, although the overall

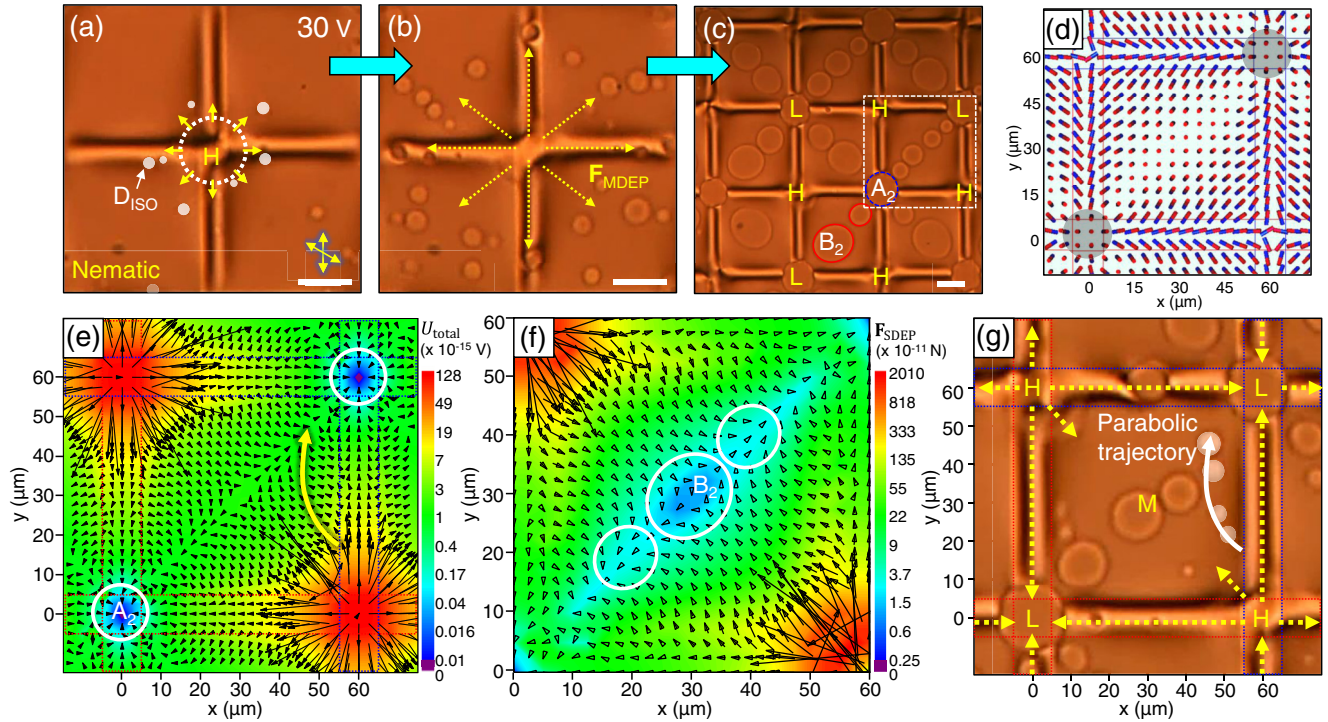


FIG. 7. (a–c) Procedure of generation, migration, and growth of isotropic droplets at 30 V. Scale bars, 20 μm . (a–b) The generation of isotropic droplets near H (the white circle) and their radial migration. (c) Diagonally aligned droplets after stopping the migration (see Supplemental Video S2 [38]). (d) LC director profile, (e) F_{SDEP} vector fields (arrows), ΔU_{total} profile (background color), and (f) the magnitude of F_{SDEP} (background color). (g) Isotropic droplet migration trajectories (yellow dotted and white solid lines).

profiles of \mathbf{E} and ∇E^2 are similar, the magnitudes of these are different at 15 and 30 V. Similarly, the magnitudes of F_{SDEP} are much higher at 30 V owing to the high applied

voltage. As a result, the speed of droplets near the M area is slower at 15 V than that at 30 V, and the traveling time from the edge to the central area is longer for the droplets

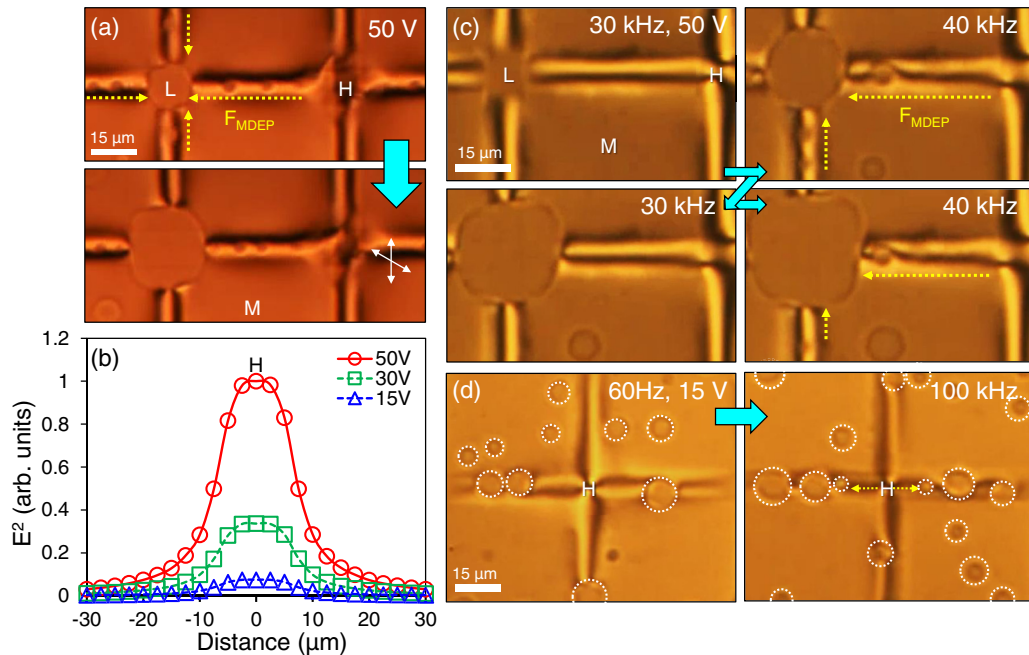


FIG. 8. (a) Generation and migration of isotropic droplets at 50 V. (b) E^2 profile across the H point, representing the relative scale of dielectric loss. (c) Droplet generation controlled by switching the frequency between 30 and 40 kHz. (d) Generation and migration of isotropic droplets at 15-V signal with the frequency of 60 Hz or 100 kHz.

at 15 V. Hence, during the slow traveling time, the droplets grow and merge together to form a large single droplet when they reach M, as shown in Fig. 6(c) and Supplemental Video S1 [38]. However, the droplets at 30 V move relatively quickly and reach the diagonal line before merging together and are likely to form the chainlike droplets along the diagonal line, as shown in Fig. 7(c) and Supplemental Video S2 [38]. Thus, the slightly different structures of the B_1 droplets at 15 V and B_2 droplets at 30 V are mainly due to the different moving speed of isotropic droplets. The diagonal chain of droplets at 30 V was rather stably sustained, but as the time went on, the B_2 droplets grew and were merged into a big droplet, similarly to B_1 droplets at 15 V.

D. SDEP at 50 V

Figures 4 and 5 show the profiles of normalized \mathbf{E} and ∇E^2 at 15, 30, and 50 V. The magnitude differences of \mathbf{E} and ∇E^2 are significant, as well indicated by the large difference of the normalization factors depending on the voltage. However, the normalized profiles are almost unchanged with the increasing voltage. This is because the variation of the effective dielectric constant of the LC is small owing to the small $\delta\epsilon$ near T_{NI} . However, the behavior of isotropic droplets is much different. At 50 V, most isotropic droplets were generated at the center of the H points, and only a few were generated outside the electrodes (Fig. 8(a) and Supplemental Video S3 [38]). The dielectric loss may be attributed to the generation of

isotropic droplets at the H points. The dielectric loss under the application of squared electric voltage increased the local temperature (T_{Local}), and is proportional to the square of the electric field (E^2) and its frequency (ν); that is, $T_{\text{Local}} \sim \nu E^2$ [41–43]. Figure 8(b) shows the relative dielectric loss along the electrode, depending on the applied voltage at 60 Hz. While the dielectric loss difference between the H point and the surrounding area is rather small for 15 V application, it increased dramatically in the case of 50 V application. The large difference could produce a large temperature gradient near the H points. At 15 V, the temperature gradient may be negligible, and the isotropic droplets appeared randomly. At 30 V, the temperature gradient is mild, and the droplets were generated around the H points. At 50 V, the temperature gradient is large and most of the droplets were generated at the H points. Thus, the generation area of the droplet is controllable to some degree by controlling the applied voltage.

The dielectric loss also depends on the frequency, and we can control the generation and location of isotropic droplets by controlling the frequency. Initially, we applied 50–V, 30-kHz signals, and then controlled the temperature of the hot stage to be roughly 0.5°C lower than the temperature in the previous experiment, so as not to generate the isotropic droplets. As shown in Fig. 8(c) and Supplemental Video S4 [38], when we increased the frequency from 30 to 40 kHz, the isotropic droplets were generated from the H point and drifted toward the L point. By controlling the frequency between

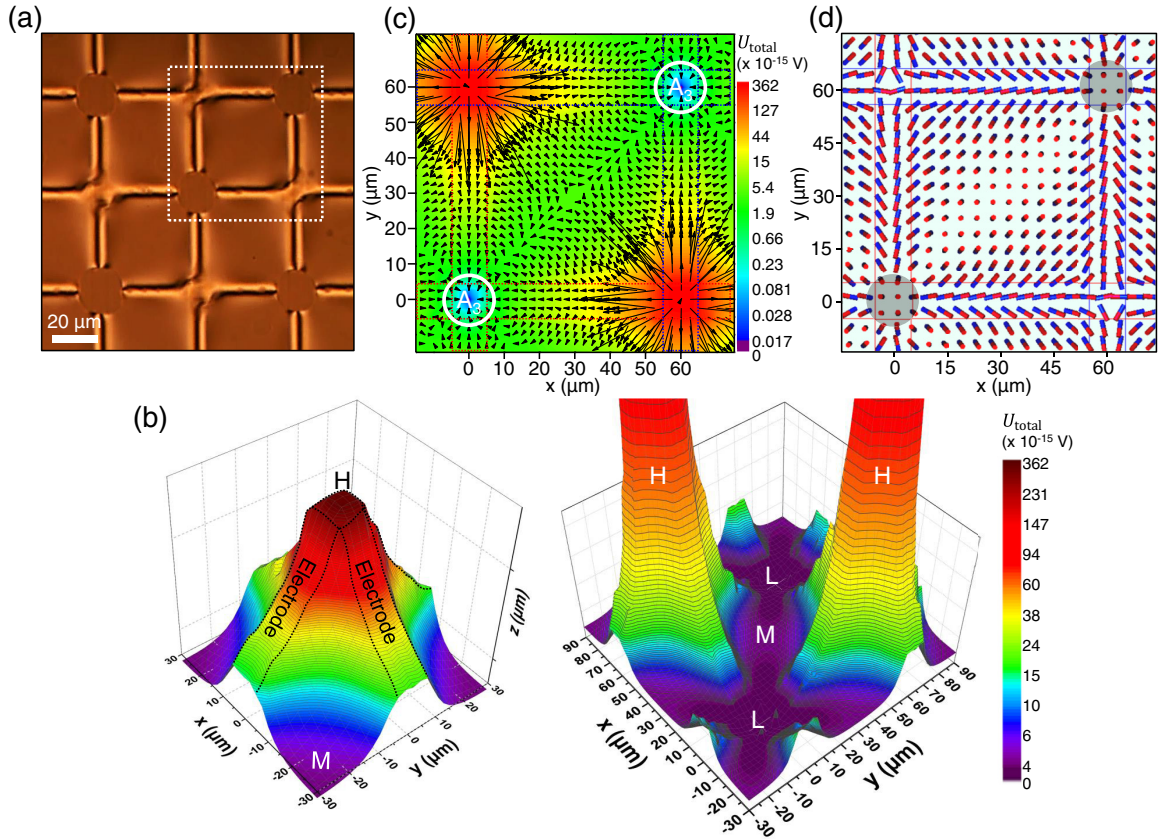


FIG. 9. (a) Periodic array of A_3 -type isotropic droplets located at the L points after stopping the droplet migration (see Supplemental Video S3 [38]). (b) ΔU_{total} profile near the H area. The left and right panels have log scale and linear scale vertical axes, respectively. (c) \mathbf{F}_{SDEP} (arrows) and ΔU_{total} profiles (background color) at 50 V. (d) LC director profile.

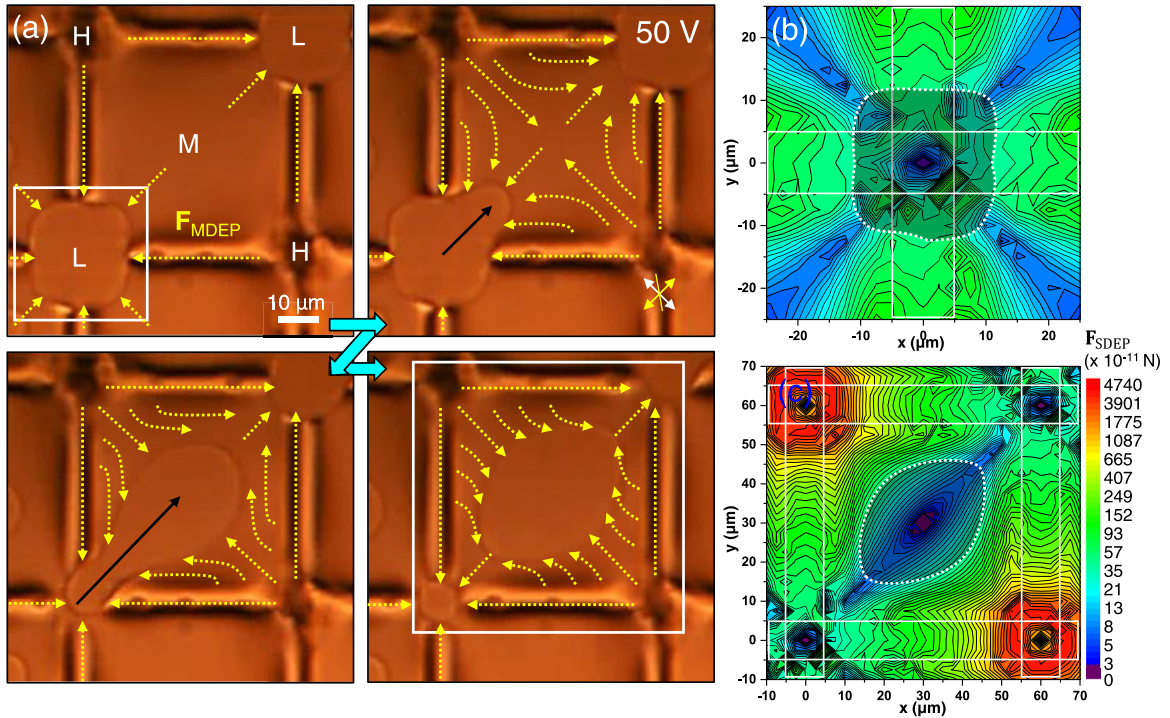


FIG. 10. (a) When the isotropic droplet grows, it is deformed, squeezed, and escapes from L to M. The yellow dotted lines represent the direction of \mathbf{F}_{MDEP} , and the black solid lines represent the moving direction of the droplet. (b) Contour lines of the magnitude of \mathbf{F}_{SDEP} around the square-shaped droplet [white box in the first image of (a)] and (c) the elliptical-shaped droplet [white box in the last image of (a)].

30 and 40 kHz, we could selectively activate or suppress the generation of isotropic droplets. Here, the threshold frequency is related to the setting value of the hot stage temperature; that is, when the setting temperature approaches T_{NI} , the threshold frequency decreases. Moreover, the location of droplet generation is controllable by changing the frequency. When the frequency of the 15-V signal was 60 Hz, the locations of isotropic droplets were random, but when the frequency was increased to 100 kHz, the isotropic droplets were mostly generated at the H points, as shown in Fig. 8(d) and Supplemental Video S5 [38].

Once isotropic droplets were generated at the center of the H points, the droplets migrated along the electrode and merged at the L points. Only a small number of droplets was generated out of the electrodes; hence, after approximately 18 s, an isotropic droplet array located at every L point was obtained, as shown in Fig. 9(a). The mechanism of droplet migration along the electrode can be understood by analyzing the ΔU_{total} profile, shown in the left image of Fig. 9(b), where the vertical axis is log scale. From the tip of the potential at the H points, four trenches are connected to the L points. As a result, the small droplets generated at the tip of the H points traveled along the trench on the electrode. The right image in Fig. 9(b) is the same ΔU_{total} profile in the linear scale, which shows more details on the low level of the potential. The traveling droplets from the H points gathered at the L points, the lowest potential points.

Figure 9(c) shows the \mathbf{F}_{SDEP} profile for 50 V; the shape of the \mathbf{F}_{SDEP} profile is almost the same as that at 30 V [Fig. 7(e)]. This is because the LC director profile is almost the same as that at 30 V [see Figs. 7(d), 9(d), and 3]. However, the droplet

distributions are very different [see Figs. 7(c) and 9(a)], which is attributed to the different locations of droplet generation at 30 and 50 V. Thus, owing to the different locations of droplet generation, different types of isotropic droplet arrays were obtained.

E. Squeezed isotropic droplet by SDEP

Because of the large local heating at the H points at 50 V, the small droplets were continuously generated at the H points and migrated to the L points, unlike the case at 30 V. Then, the droplets at the L points kept growing by consuming the small droplets from the H points. When the size of the droplet at the L points increased to a certain size, its shape was deformed to a square owing to the anisotropic SDEP pressure [the first image in Fig. 10(a)]. The ΔU_{total} profile in Fig. 9(b) clearly shows the anisotropic potential shape around the L points. As the size further increased, the droplet was further deformed [the second image] and squeezed [the third image]. Then, the isotropic droplet escaped from L to M, producing the elliptical-shaped droplet (the last image in Fig. 10(a) and Supplemental Video S6 [38]). Here, the interesting point is that the lowest potential point is the L point, and the direction of \mathbf{F}_{SDEP} is from M to L [see the yellow dotted arrows in Fig. 10(a)]. However, owing to the squeezing force along the electrodes near the L point, the isotropic droplet cannot stably reside at the L point, and escapes to the M region with relatively higher potential and weaker force. Figure 10(b) shows the contour lines of the magnitude of \mathbf{F}_{SDEP} , demonstrating the squeezing force near the L points. The shape of the droplet in the middle of the compartment matches well with the contour lines of the magnitude of \mathbf{F}_{SDEP} [Fig. 10(c)].

IV. CONCLUSIONS

We investigated the SDEP phenomena of isotropic droplets in an LC cell with cross-shaped electrodes at different applied voltages. We identified several important factors in the SDEP of isotropic droplets. First, the generation location of isotropic droplets is related to the dielectric loss profile and resulting temperature profile in the cell. Thus, as the applied voltage increased, the locations of isotropic droplet generation were localized close to the H point, where the electric fields were strongest. The underlying mechanism is related to the dielectric loss depending on the square of the electric fields and the resulting temperature gradient. Second, the moving trajectories of isotropic droplets are significantly influenced by their generation location. For example, the droplets generated at the H point and on electrodes drifted along the elec-

trodes, but other droplets moved toward the central area of the compartment enclosed by electrodes. The detailed migration trajectories of the droplets were also well matched with the theoretical profile of \mathbf{F}_{SDEP} and ΔU_{total} profile. Third, the shape of the isotropic droplet arrays depends on the applied voltage. Finally, when an isotropic droplet is squeezed by nonuniform \mathbf{F}_{SDEP} force, the droplet can be deformed and escape from the squeezing area. These results are expected to improve the understanding of SDEP.

ACKNOWLEDGMENT

This work was supported by the National Research Foundation of Korea (NRF) funded by the Ministry of Science and ICT (Grant No. NRF2019R1A2C2008359).

- [1] T. B. Jones and T. B. Jones, *Electromechanics of Particles* (Cambridge University Press, Cambridge, 2005).
- [2] P. R. C. Gascoyne and J. Vykoukal, *Electrophoresis* **23**, 1973 (2002).
- [3] H. A. Pohl, K. Pollock, and J. S. Crane, *J. Biol. Phys.* **6**, 133 (1978).
- [4] R. Pethig, H. Ying, W. Xiao-bo, and J. P. H. Burt, *J. Phys. D* **25**, 881 (1992).
- [5] B. R. Burg, F. Lütolf, J. Schneider, N. C. Schirmer, T. Schwamb, and D. Poulikakos, *Appl. Phys. Lett.* **94**, 053110 (2009).
- [6] B. Singh, J. Wang, S. Rathi, and G.-H. Kim, *Appl. Phys. Lett.* **106**, 203106 (2015).
- [7] J. J. Boote and S. D. Evans, *Nanotechnology* **16**, 1500 (2005).
- [8] A. D. Wissner-Gross, *Nanotechnology* **17**, 4986 (2006).
- [9] S. Choi *et al.*, *Anal. Chem.* **88**, 10867 (2016).
- [10] I. S. Park *et al.*, *ACS Nano* **10**, 4011 (2016).
- [11] S. I. Han, H. Soo Kim, and A. Han, *Biosens. Bioelectron.* **97**, 41 (2017).
- [12] J. R. Millman, K. H. Bhatt, B. G. Prevo, and O. D. Velev, *Nat. Mater.* **4**, 98 (2005).
- [13] B. Lee, J.-S. Lee, and J.-K. Song, *Soft Matter* **15**, 5026 (2019).
- [14] J.-H. Son, S.-D. Kim, J. K. Vij, and J.-K. Song, *Appl. Phys. Lett.* **105**, 251601 (2014).
- [15] S.-D. Kim, B. Lee, S.-W. Kang, and J.-K. Song, *Nat. Commun.* **6**, 7936 (2015).
- [16] S. Aya, Y. Sasaki, F. Araoka, K. Ema, K. Ishikawa, A. V. Emelyanenko, and H. Takezoe, *Phys. Rev. Lett.* **106**, 117801 (2011).
- [17] C.-p. Fan and M. J. Stephen, *Phys. Rev. Lett.* **25**, 500 (1970).
- [18] S.-D. Kim, J.-K. Guo, and J.-K. Song, *Liq. Cryst.* **43**, 1237 (2016).
- [19] C. Völtz and R. Stannarius, *Phys. Rev. E* **70**, 061702 (2004).
- [20] M. Škarabot, Ž. Lokar, and I. Muševič, *Phys. Rev. E* **87**, 062501 (2013).
- [21] J. L. West, A. Glushchenko, G. Liao, Y. Reznikov, D. Andrienko, and M. P. Allen, *Phys. Rev. E* **66**, 012702 (2002).
- [22] O. D. Lavrentovich, *Soft Matter* **10**, 1264 (2014).
- [23] J. L. West, K. Zhang, A. Glushchenko, D. Andrienko, M. Tasinkevych, and Y. Reznikov, *Eur. Phys. J. E* **20**, 237 (2006).
- [24] J.-S. Lee, B. Lee, S.-H. Song, and J.-K. Song, *Part. Part. Syst. Charact.* **36**, 1800470 (2019).
- [25] K. D. Barbee, A. P. Hsiao, E. E. Roller, and X. Huang, *Lab Chip* **10**, 3084 (2010).
- [26] J. R. Webster, M. A. Burns, D. T. Burke, and C. H. Mastrangelo, *Anal. Chem.* **73**, 1622 (2001).
- [27] E. Sollier, C. Murray, P. Maoddi, and D. Di Carlo, *Lab Chip* **11**, 3752 (2011).
- [28] C.-F. Chen, J. Liu, C.-C. Chang, and D. L. DeVoe, *Lab Chip* **9**, 3511 (2009).
- [29] L. Y. Yeo, H.-C. Chang, P. P. Y. Chan, and J. R. Friend, *Small* **7**, 12 (2011).
- [30] J. P. Huang, M. Karttunen, K. W. Yu, and L. Dong, *Phys. Rev. E* **67**, 021403 (2003).
- [31] A. Kuzyk, *Electrophoresis* **32**, 2307 (2011).
- [32] H. Zhou, M. A. Preston, R. D. Tilton, and L. R. White, *J. Colloid. Interface Sci.* **285**, 845 (2005).
- [33] A. Dalili, E. Samiei, and M. Hoorfar, *Analyst* **144**, 87 (2019).
- [34] S. Park, Y. Zhang, T.-H. Wang, and S. Yang, *Lab Chip* **11**, 2893 (2011).
- [35] H. D. Xi *et al.*, *Lab Chip* **17**, 751 (2017).
- [36] J.-K. Guo, J. K. Vij, and J.-K. Song, *Adv. Opt. Mater.* **5**, 1700119 (2017).
- [37] J.-K. Guo, S.-H. Hong, H.-J. Yoon, G. Babakhanova, O. D. Lavrentovich, and J.-K. Song, *Adv. Sci.* **6**, 1900785 (2019).
- [38] See Supplemental Material at <http://link.aps.org/supplemental/10.1103/PhysRevE.101.012704> for the videos of the behaviors of isotropic droplets at 15 V, 30 V, and 50 V, and at 30 kHz, 40 kHz, and 100 kHz, and the videos of a squeezed isotropic droplet by SDEP pressure.
- [39] A. Rohani, B. J. Sanghavi, A. Salahi, K. T. Liao, C. F. Chou, and N. S. Swami, *Nanoscale* **9**, 12124 (2017).
- [40] S. Park, M. Koklu, and A. Beskok, *Anal. Chem.* **81**, 2303 (2009).
- [41] G. Kuznetsov, E. Kravchenko, and N. Pribaturin, *J. Commun. Technol. Electron.* **63**, 381 (2018).
- [42] M. Schadt, *Mol. Cryst. Liq. Cryst.* **66**, 319 (1981).
- [43] Y. Yin, S. V. Shiyankovskii, and O. D. Lavrentovich, *J. Appl. Phys.* **100**, 024906 (2006).